

Expansion of Bose-Hubbard Mott insulators in optical lattices

Mark Jreissaty,¹ Juan Carrasquilla,¹ F. Alexander Wolf,^{1,2} and Marcos Rigol¹

¹*Department of Physics, Georgetown University, Washington, DC 20057, USA*

²*Theoretical Physics III, Center for Electronic Correlations and Magnetism, Institute of Physics, Augsburg University, D-86135 Augsburg, Germany*

We study the expansion of bosonic Mott insulators in the presence of an optical lattice after switching off a confining potential. We use the Gutzwiller mean-field approximation and consider two different setups. In the first one, the expansion is restricted to one direction. We show that this leads to the emergence of two condensates with well defined momenta, and argue that such a construct can be used to create atom lasers in optical lattices. In the second setup, we study Mott insulators that are allowed to expand in all directions in the lattice. In this case, a simple condensate is seen to develop within the mean-field approximation. However, its constituent bosons are found to populate many nonzero momentum modes. An analytic understanding of both phenomena in terms of the exact dispersion relation in the hard-core limit is presented.

PACS numbers: 03.75.Kk,03.75.-b,03.75.Hh,05.30.Jp

I. INTRODUCTION

In recent years, the study of strongly correlated ultracold gases in optical lattices has become an important focus of experimental and theoretical research [1, 2]. Initially, many of the efforts were devoted to studying equilibrium quantum phase transitions, for which the observation of the superfluid to Mott-insulator phase transitions in three [3], two [4], and one [5] dimension was a major experimental accomplishment. More recently, the study of the nonequilibrium dynamics of these systems has started gaining attention [6–10]. The latter is possible, and offers great insights into the coherent dynamics of quantum systems, thanks to the nearly ideal isolation of the gas from the environment, and to the unique control that has been achieved experimentally over the parameters that determine the dynamics.

The nonequilibrium dynamics of quantum systems is a rich subject; see, e.g., Refs. [11–13]. In this paper, we will be mainly interested in the expansion of a strongly interacting bosonic gas in the presence of an optical lattice. Experimentally, expansions (time-of-flight measurements) have been used to learn about the properties of equilibrium gases [14]. The idea behind those measurements is that, if the gas is allowed to expand in the absence of interactions, the initial momentum distribution function fully determines the density distribution after a long expansion time. Hence, by taking a picture of the latter, one can determine the former by means of a simple rescaling [1, 2, 14]. In such experiments, the particles are allowed to expand in absence of both the trapping potential and the underlying optical lattice. This implies that the kinetic energy is significantly larger than the interaction energy and, therefore, interactions can generally be neglected during the expansion. On the other hand, in the presence of the optical lattice where interactions cannot be neglected during the expansion, unusual phenomena can occur [15], e.g., the transformation of the momentum distribution of an expanding gas of impenetrable bosons into the momentum distribution function

of a noninteracting Fermi gas in equilibrium, which has a Fermi edge [16, 17]. In addition, it has been recently proposed that the expansion of two-component fermions in the presence of strong interactions in an optical lattice can be used as a tool to cool the gas through a “quantum distillation” process [18].

There is another remarkable phenomenon that occurs during the expansion of a strongly interacting gas of bosons in an optical lattice, and that is the emergence of coherence during the expansion of Mott-insulating states. This phenomenon will be the main focus of the present paper. A Mott insulator is an interaction-generated insulator that exhibits a gap to one-particle excitations. The presence of this gap produces an exponential decay of the one-particle correlations. Within the Bose-Hubbard model description, the Mott insulator is the ground state of lattice bosons for commensurate fillings and sufficiently strong interactions [19]. As mentioned before, Mott insulators have been created experimentally using ultracold gases in optical lattices. Due to the presence of a trapping potential, the Mott insulating phases in experiments usually coexist with superfluid domains. Surprisingly, when Mott insulators are allowed to expand by turning off the trap in the presence of a lattice, coherence emerges between initially uncorrelated particles [20–22], a phenomenon that resembles a sort of dynamical phase transition.

The study in Ref. [20] demonstrated that the expansion of pure Mott-insulating states of hard-core bosons in one dimension (1D) leads to the development of quasi-long-range correlations and to the emergence of quasi-condensates at finite momenta $k = \pm\pi/2a$ (where a is the lattice parameter). In a related setup, the onset of quasi-long-range correlations has been studied more recently (in the spin-1/2 language) using various analytic and approximate approaches [23]. It is important to note that these results were obtained in the limit of infinite on-site repulsions between the bosons (hard-core limit), and for pure Mott-insulating domains. It is, therefore, natural to wonder whether the same results can be ob-

served experimentally with ultracold gases, for which the on-site interactions are not infinite and the insulating domains are always surrounded by superfluid ones. Systems containing hard-core bosons, in which superfluid and insulating domains coexist, were studied in Ref. [21]. It was found there that, if most of the initial system is in a Mott-insulating state, quasicondensates with momenta $k \approx \pm\pi/2a$ are generated. The superfluid wings surrounding the insulating domain in the initial density profiles appeared to have no negative effect on the emergence of quasicohherence during the expansion. Furthermore, the expansion of a Mott insulator in a system with finite on-site interactions (soft-core bosons) was studied in Ref. [22]. Once again, quasi-long-range coherence developed during the expansion and lead to quasicondensates with momenta $|k| \lesssim \pi/2a$. The differences between the position of the peaks for soft-core bosons and hard-core bosons can be understood by considering their respective dispersion relations. Finally, a similar onset of power-law decaying correlations has been observed during the expansion of a Mott insulator within the fermionic Hubbard model [24].

A more challenging question is what happens in higher dimensions. This question poses greater conceptual and computational challenges. Since hard-core bosons in 1D are described by an integrable model, one may expect their behavior to be unique. Hence it may not extend to nonintegrable models far from any integrable limit, such as the Bose-Hubbard model with finite on-site interaction in higher dimensions. In the particular case of one spatial dimension, since the boson's on-site interaction has to be strong enough for a Mott insulator to exist, the results obtained for the 1D expansion [22] can be thought as still affected by the infinite-repulsion integrable limit, and thus may not generalize to higher dimensions. Furthermore, while the 1D expansion can be studied by means of exact analytical and/or numerical approaches in the hard-core limit [20, 21, 23] and by means of an unbiased numerical technique for the soft-core case (the time-dependent-density-matrix-renormalization-group approach [25]), no such tool exists to study the expansion in higher dimensions. For the latter, no efficient and unbiased, analytical, or computational approach is known that can deal with the dynamics in the presence of strong interactions. Approximations are therefore required to study these systems.

A first step toward understanding what happens in higher dimensions was taken in Ref. [26]. In that work, which was a study in the hard-core limit utilizing the Gutzwiller mean-field approximation, a three-dimensional (3D) Mott insulator was allowed to expand in a single direction in the lattice. The study showed that condensates emerge at finite momenta following the “melting” of a Mott insulator. In addition, the momenta of the resulting condensates were found to be fully determined by the ratio between the hopping amplitudes transverse to and along the expansion. Hence these systems can be used to create highly controllable atom

lasers. Other nonequilibrium setups that allow one to obtain condensation at finite momentum [27, 28] do not seem suitable for the latter purpose.

In this paper, we extend the results reported in Ref. [26] to the expansion of Mott insulators with finite on-site interaction in two dimensions (2D). Our results in 2D can be straightforwardly extended to three dimensions. We first consider a setup similar to that in Ref. [26], in which soft-core bosons are allowed to expand in a single direction. We show that similarly to the case in the hard-core limit, condensates emerge at finite momenta. We then proceed to study a system in which the Mott insulator is allowed to expand in all directions of the lattice. For this particular case, we show that, at least within the mean-field approximation, a simple condensate with many different momenta develops as the Mott insulator expands. We also discuss how these results can be understood in terms of the exact dispersion relation in the hard-core limit.

The paper is organized as follows. In Sec. II, we introduce the model and the time-dependent mean-field approach used to study the expansion. The explanation of how our initial states are prepared is presented in Sec. III. Section IV is devoted to the study of the expansion along one direction. The case in which the Mott insulator is allowed to expand in all directions is discussed in Sec. V. Finally, the conclusions are presented in Sec. VI.

II. MODEL AND MEAN-FIELD APPROACH

Our study is relevant to ultracold bosons trapped in deep optical lattices. They can be well described by the Bose-Hubbard Hamiltonian [29]

$$\hat{H} = - \sum_{\langle i,j \rangle} J_{ij} \left(\hat{a}_i^\dagger \hat{a}_j + \text{H.c.} \right) + \frac{U}{2} \sum_i \hat{n}_i (\hat{n}_i - 1) + \sum_i (V_x x_i^2 + V_y y_i^2) \hat{n}_i, \quad (1)$$

where \hat{a}_i^\dagger (\hat{a}_i) is the boson creation (annihilation) operator at a given site i , and $\hat{n}_i = \hat{a}_i^\dagger \hat{a}_i$ is the particle number operator. The first two terms of the expression are the usual kinetic and interaction terms that define the Hubbard model in the homogeneous case, where J_{ij} is the hopping amplitude between neighboring sites i and j ($\langle i, j \rangle$), and U is the on-site interaction strength. In experiments involving ultracold gases, a trap is required to confine the atoms. To a good approximation, those traps are harmonic, as considered in the last term in Eq. (1). Here, V_x and V_y denote the strength of the trap in the x and y direction, while x_i and y_i are the coordinates of site i with respect to the center of the trap. In the remainder of the manuscript, positions will be given in units of the lattice spacing a , which is taken to be the same in all directions.

The ground-state phase diagram of the homogeneous case ($V_x = V_y = 0$ and $J_{ij} = J$) has been studied exten-

sively in all dimensions [19, 30–35]. As mentioned earlier, it contains both superfluid and Mott-insulating phases. The former occurs for incommensurate fillings, and for commensurate fillings for U/J is below some critical value that depends on the filling and dimensionality of the system. The insulating phases are only present for commensurate fillings and sufficiently strong interactions. This model is not exactly solvable in any dimension. Unbiased results for the phase diagram have been obtained using quantum Monte Carlo simulations [30, 34, 35], density-matrix renormalization group (1D) [33], and strong coupling expansions [31, 32]. Interestingly, a simple approximation such as the Gutzwiller mean-field theory, which is exact only in the limit of infinite dimensions, can still describe qualitatively the complete phase diagram of this model for finite dimensions [19].

In the presence of a trap, superfluid and Mott-insulating phases coexist and form a “wedding cake” structure [36–38]. The particular shape of the density distribution function can be understood within the local density approximation [1], given the phase diagram in the homogeneous case (see Fig. 1, and the accompanying explanation). Experimentally, such a structure has been observed by several groups [39–43]. As mentioned in the Introduction, the unique opportunities provided by the study of these systems come from the experimentalist’s high degree of control over the depth and structure of the optical lattice and the confining potential. Essentially, all the microscopic parameters in Eq. (1) can be manipulated and made time dependent. For example, J , U , and V_x, V_y can be modified by changing the intensity of the laser beams that produce the lattice; V_x, V_y can be modified by introducing an additional trapping (or antitrapping) magnetic field; and U can be modified using Feshbach resonances. Together with the high degree of isolation from the environment, this level of control makes these experiments ideal to study the effects of strong correlations and dimensionality in the nonequilibrium dynamics of the expanding gases.

In this paper, we are interested in studying the expansion of Mott-insulating states in the lattice. For this, we prepare the system in its ground state, for a particular number of particles, U , J , and V_x, V_y . At time $t = 0$, we turn off the trap and allow the system to expand in the presence of the optical lattice. During the expansion, particles interact strongly and we compute observables such as the density, momentum distribution function, and condensate fraction, as a function of time. All our calculations are performed utilizing the time-dependent Gutzwiller mean-field theory. This is a good approximation in high dimensions and, in Ref. [26], it was shown to qualitatively reproduce the behavior seen in an exact diagonalization study of the expansion in (small) 2D lattices.

This mean-field theory is based on the restriction that

the wave function is of the Gutzwiller-type product state,

$$|\Psi_{\text{MF}}\rangle = \prod_{i=1}^L \sum_{n=0}^{n_c} \gamma_{in} |n\rangle_i, \quad (2)$$

where L is the number of lattice sites, n_c is a cutoff taken to be large enough such that all our results are independent of n_c ($n_c = 3$ in our calculations), $|n\rangle_i$ are the Fock states for lattice site i , and the complex coefficients γ_{in} are variational parameters determined by minimizing the expectation value

$$\langle \Psi_{\text{MF}} | \hat{H} - \mu \hat{N} | \Psi_{\text{MF}} \rangle. \quad (3)$$

In Eq. (3), μ is the chemical potential, i.e., we work on the grand canonical ensemble, and \hat{N} the total number of particle operator.

The energy minimization leads to the set of equations

$$\sum_{\langle j \rangle_i} -J_{ij} [\sqrt{n+1} \gamma_{i(n+1)} \Phi_j^* + \sqrt{n} \gamma_{i(n-1)} \Phi_j] + n \left[\frac{U}{2}(n+1) + V_i - \mu \right] \gamma_{in} = 0, \quad (4)$$

where $\sum_{\langle j \rangle_i}$ denotes a summation over all j that are nearest neighbors of i , $V_i = V_x x_i^2 + V_y y_i^2$, and $\gamma_{i(-1)} = \gamma_{i(n_c+1)} = 0$. The mean-field Φ_j is defined as

$$\Phi_j = \langle \hat{a}_j \rangle = \sum_{n=1}^{n_c} \sqrt{n} \gamma_{j(n-1)}^* \gamma_{jn}. \quad (5)$$

By solving Eq. (4), one obtains all the coefficients γ_{in} in Eq. (2), and hence determines the initial state for the time evolution.

An alternative approach, which is equivalent to that of solving Eq. (4), can be used. It consists in finding the ground state of the following mean-field decoupled Hamiltonian [44]:

$$\hat{\mathcal{H}}_{\text{MF}} = - \sum_{\langle i,j \rangle} J_{ij} \left(\hat{a}_i^\dagger \Phi_j + \Phi_i^* \hat{a}_j - \Phi_i^* \Phi_j \right) + \text{H.c.} + \frac{U}{2} \sum_i \hat{n}_i (\hat{n}_i - 1) + \sum_i (V_i - \mu) \hat{n}_i. \quad (6)$$

This Hamiltonian is obtained by a decoupling of the hopping terms in Eq. (1) as

$$\hat{a}_i^\dagger \hat{a}_j \simeq \hat{a}_i^\dagger \Phi_j + \hat{a}_j \Phi_i^* - \Phi_i^* \Phi_j. \quad (7)$$

Equation (1) can then be written as a sum over single-site Hamiltonians $\hat{\mathcal{H}}_i$, coupled only through constant neighboring terms Φ_j . This implies that the ground state of the decoupled Hamiltonian can be written as the product state in Eq. (2). The optimal set of coefficients γ_{in} is related to the ground-state eigenvector components of the Hamiltonian in Eq. (6) subject to the condition in Eq. (5), which has to be self-consistently satisfied. In

practice, this condition is reached as follows: an arbitrary set of nonzero Φ_i^0 is used to construct a set of decoupled Hamiltonians $\hat{\mathcal{H}}_i$ which are diagonalized for each site in order to obtain a set of γ_{in} 's. Given γ_{in} , a set of Φ_i^{new} is computed according to Eq. (5). If the elements on this new set are equal to those of the previous set Φ_i^0 within a certain desired precision, then self-consistency has been reached. If not, we set $\Phi_i^0 = \Phi_i^{\text{new}}$ and construct a new set of decoupled Hamiltonians and the process of diagonalizing and finding Φ_i^{new} is iteratively repeated until self-consistency is satisfied. We have verified that both approaches based on Eq. (4) and Eq. (6) provide quantitatively consistent results. However, at least within our implementations, the one based on the mean-field decoupled Hamiltonian is more stable and considerably faster than the one based on the direct solution of Eq. (4).

After turning off the trap, the time evolution of $|\psi_{\text{MF}}\rangle$ is computed using the time-dependent variational principle [45–48], which minimizes the expectation value,

$$\langle \Psi_{\text{MF}} | i\partial_t - \hat{H} + \mu\hat{N} | \Psi_{\text{MF}} \rangle, \quad (8)$$

and leads to the following set of differential equations:

$$i\dot{\gamma}_{in} = - \sum_{\langle j \rangle_i} J_{ij} [\sqrt{n+1} \gamma_{i(n+1)} \Phi_j^* + \sqrt{n} \gamma_{i(n-1)} \Phi_j] + n \left[\frac{U}{2}(n-1) + V_i - \mu \right] \gamma_{in}. \quad (9)$$

Here, we use the same notation as in Eq. (4). It is important to note that Eq. (9) determines the time evolution while preserving the normalization of the wave function and the total number of particles N_b in the system. We solve this set of $L \times (n_c + 1)$ differential equations numerically, using a fourth-order Runge-Kutta method. Self-consistency is enforced by monitoring the total energy, particle number, and the normalization.

III. THE INITIAL STATE

We are interested in the expansion of Mott-insulating states, though we know *a priori* that, in presence of a trapping potential, such Mott states are inevitably surrounded by superfluid regions. Nevertheless, one can aim at finding a setup for which those Mott domains are as large as possible for a given value of J/U . Our approach to achieving large Mott domains is based on the local-density approximation (LDA). The LDA assumes that the local properties of the confined system can be mapped to those properties of the homogeneous system with the same value of J/U and an effective chemical potential corresponding to the spatially varying $\mu_i = \mu - V_i$ at site i in the trap. One can, therefore, get an approximate picture of what the trapped system looks like based on the phase diagram of the homogeneous system. Within the LDA, in order to get the largest Mott domain, it is enough to set the chemical potential at the center of

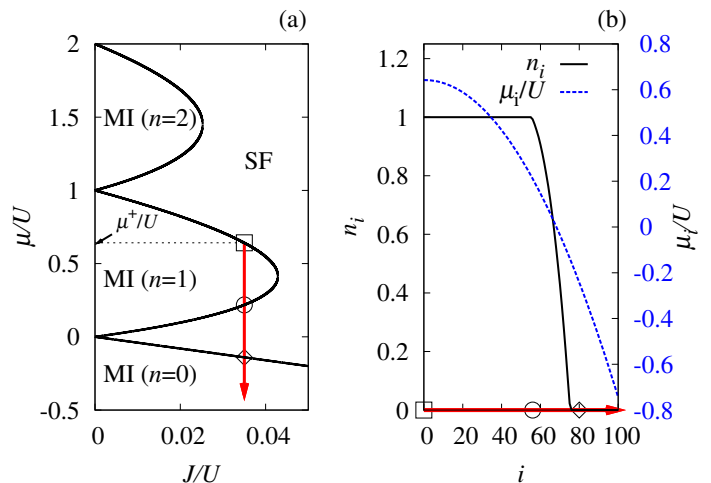


FIG. 1. (Color online) (a) Mean-field phase diagram of the Bose-Hubbard model in 2D. The red arrow follows the different phases occurring in the trapped system as one moves away from the center of the trap. (b) The density profile as obtained from the LDA with the largest Mott domain plotted together with the spatially varying chemical potential μ_i/U .

the trap to be the largest chemical potential of the homogeneous system that allows for a Mott insulator with density $n = 1$. That is just the value of the chemical potential μ^+ right at the transition from the Mott insulator with density $n = 1$ to the superfluid with $n > 1$. This is based on the observation that, as the distance from the center of the trap is increased, the effective chemical potential of the homogeneous system decreases. In 2D, the critical value μ^+ can be determined within the mean-field theory by finding the largest solution for μ from the following relation that determines the boundaries of the Mott lobes [49],

$$\frac{2(J_x + J_y)}{U} = \frac{(n - \mu/U)(\mu/U - n + 1)}{1 + \mu/U}, \quad (10)$$

where J_x and J_y are the hopping parameters along the x and y directions, respectively. These ideas are illustrated in Fig. 1, where the mean-field phase diagram of the homogeneous 2D system is depicted [Fig. 1(a)], as well as the density profile across the center of a trapped system that contains the largest Mott domain as obtained from the LDA [Fig. 1(b)].

We should stress that, once μ^+ has been identified, we select a value of μ close to μ^+ and solve Eq. (4) and/or Eq. (6) to obtain the initial state. Hence our initial state is always the exact ground state within the mean-field approximation, i.e., it is not the LDA ground state. This is the way the initial wave function in Eq. (2) is constructed for all our expansions.

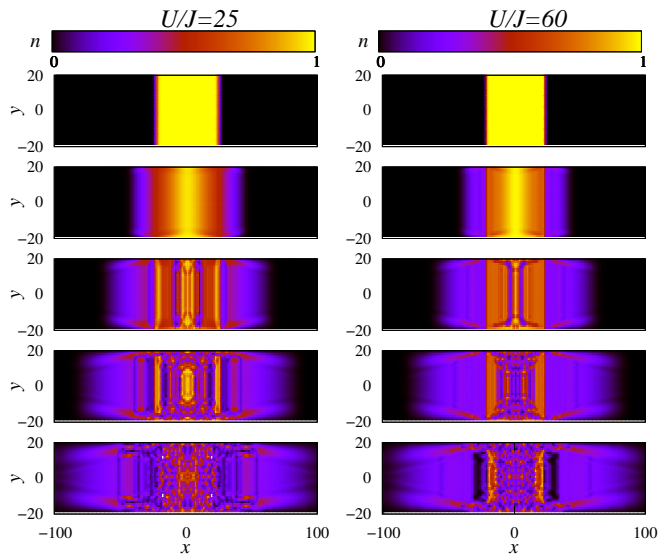


FIG. 2. (Color online) Comparison between the time evolution of the density profile across the trap of systems with $U/J_x = 25$ (left) and $U/J_x = 60$ (right), at $t = 0, 10, 20, 30$ and 40 (from top to bottom) following the release from traps with $V_x/J_x = 0.03$ and $V_x/J_x = 0.08$, respectively. $\eta = 0.3$ and the time is reported in units of \hbar/J_x .

IV. EXPANSION IN ONE DIRECTION

Let us first consider the expansion of a Mott insulator along one direction in the lattice. We study the case in which the initial state is confined only along the x direction, i.e., $V_y = 0$, while V_x is kept finite, but the system has open boundary conditions in the y direction (a box trap). We allow for the hopping amplitudes to be anisotropic, namely, that the hopping along the x direction (J_x) differs from the one along the y direction (J_y). We then study the expansion for several values of U/J_x , large enough so that the Mott-insulating phase exists, as well as different values of $\eta = J_y/J_x$. In all cases considered in this section, the expansion takes place in a lattice with 200×40 sites. As stated in the Introduction, this study extends the results presented in Ref. [26] on the expansion of hard-core bosons in three-dimensional lattices to the expansion of soft-core bosons confined in two-dimensional lattices. The initial state is selected such that the Mott-insulating domain is the largest possible for given values of U/J_x , η , and V_x/J_x , as explained in the previous section.

In Fig. 2, we show the time evolution of the density profiles of systems with $U/J_x = 25$ and 60 , for $\eta = 0.3$. In the initial state ($t = 0$), both systems exhibit large Mott-insulating domains in the center of the lattice ($x = 0$), surrounded by small superfluid regions, the latter being larger for the smallest interaction strength, i.e., $U/J_x = 25$. For $t > 0$, the particles are allowed to expand by switching off the confining potential along the x direction. As a result, the Mott-insulating domains melt. This process is seen to be qualitatively similar for the two

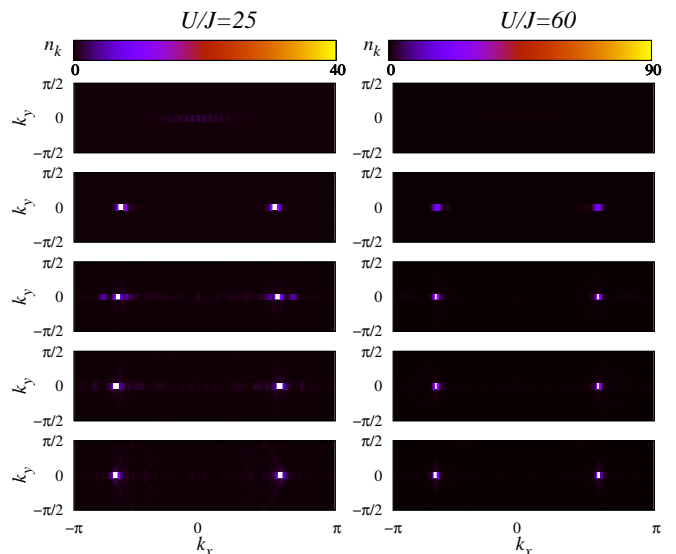


FIG. 3. (Color online) Comparison between the time evolution of the momentum distribution function of systems with $U/J_x = 25$ (left) and $U/J_x = 60$ (right), at $t = 0, 10, 20, 30$ and 40 (from top to bottom) following the release from traps with $V_x/J_x = 0.03$ and $V_x/J_x = 0.08$, respectively. $\eta = 0.3$ and the time is reported in units of \hbar/J_x .

values of U/J_x considered in Fig. 2. Note that during the time evolution, due to the symmetry of the initial state, the system expands only along the x direction, and the density profile maintains the reflection symmetry with respect to both x and y axes.

The corresponding momentum distributions $n_{\mathbf{k}}$ of the systems we have just described are presented in Fig. 3. At $t = 0$, although barely observable in the plots (first row in Fig. 3), there is a sizable population of low momentum modes, because of the presence of the inevitable superfluid regions surrounding the initial Mott insulators. Those modes are embedded in a roughly homogeneous background of low-populated momenta. The latter are the result of the large Mott-insulating domains present in the initial states (top panels in Fig. 2). Remarkably, shortly after the expansion has started, particles get redistributed in momentum space, and they tend to fill up states surrounding two well-defined momentum values $\mathbf{k} = (\pm k_x^*, 0)$. This effect, which can be clearly observed in all panels with $t > 0$ in Fig. 3, is already present at very early times $t < 10$. As the expansion goes on, the values of the momentum of the highly populated modes become time independent. Their finite momenta reflects the motion of the two groups of particles moving away from the center of the systems in Fig. 2. We find that the structure around the momentum peaks, better seen in the left column in Fig. 3 around \mathbf{k} , disappears as the value of U/J_x is increased, and only sharp peaks are left. This is apparent by comparing the momentum distribution functions between $t = 20$ and $t = 40$ in Fig. 2. There, the peaks for $U/J_x = 60$ are much sharper than those for $U/J_x = 25$.

To a very good approximation, one can predict the values of \mathbf{k} seen in Fig. 3 using energy and momentum conservation arguments. In order to do that, we first realize that, if U/J_x is large enough, double or higher occupancies of the lattice sites become energetically too costly and can be, to a first approximation, ignored. The system can then be thought as composed of hard-core bosons. Following Ref. [26], the kinetic energy can then be written as

$$E_{\text{kin}} = \sum_{\mathbf{k}} \epsilon_{\mathbf{k}} n_{\mathbf{k}}, \quad (11)$$

where $n_{\mathbf{k}}$ is the momentum distribution function at any given time, $\mathbf{k} = (k_x, k_y)$, and $\epsilon_{\mathbf{k}}$ is the dispersion relation

$$\epsilon_{\mathbf{k}} = -2J_x \cos k_x - 2J_y \cos k_y. \quad (12)$$

In order to further simplify the calculations, one can assume that the system before the expansion is a pure Mott insulator, thus neglecting the small superfluid regions that are always present in the trap, and implying that the initial kinetic energy is $E_{\text{kin}} \approx 0$. (Note that if double occupancies are neglected, the kinetic energy is essentially the total energy of the system after the trap has been turned off.) We further recall the observation that, in Fig. 3, many particles tend to populate modes with $\mathbf{k} = (\pm k_x^*, 0)$, from which we understand that the y component of \mathbf{k} is zero due to the symmetry of the expansion, which occurs only along the x direction. We can now ask, within our simplified picture of the systems presented in Figs. 2 and 3, which modes [with $(k_x^*, 0)$] could be populated by all the particles after the expansion while still conserving the energy. (We are assuming that interactions during the expansion redistribute the energy in such a way that all particles condense into a single mode.) From Eq. (11), it follows that

$$\cos k_x^* = -\eta. \quad (13)$$

If, in addition to energy conservation, we enforce conservation of the total lattice momentum, or the symmetry of the expansion for that matter, we conclude that $\mathbf{k} = (\pm k_x^*, 0)$, where $k_x^* = \arccos(-\eta)$.

From Eq. (13), it follows that, in the limit of $U/J_x \gg 1$, the location of the \mathbf{k} modes that are populated during the expansion depends only on the ratio η . Remarkably, we find that the peaks in Fig. 3 agree very well with that prediction [Eq. (13)]. This occurs despite the fact that, in Fig. 3, the results were obtained for finite values of U/J_x and in the presence of small superfluid domains around the Mott insulator. In Fig. 4(a), we report a complete study of the dependence of the location of the peaks in the mean-field calculations as a function of η , for three values of U/J_x (points), together with the predictions of Eq. (13) (solid line). For the smallest values of U/J_x that allow for the realization of a Mott insulator, one expects some dependence of the location of the peaks on U/J_x , because the dispersion relation is expected to exhibit the largest differences from Eq. (12). The deviations of the mean-field results from Eq. (13) are, however, very small

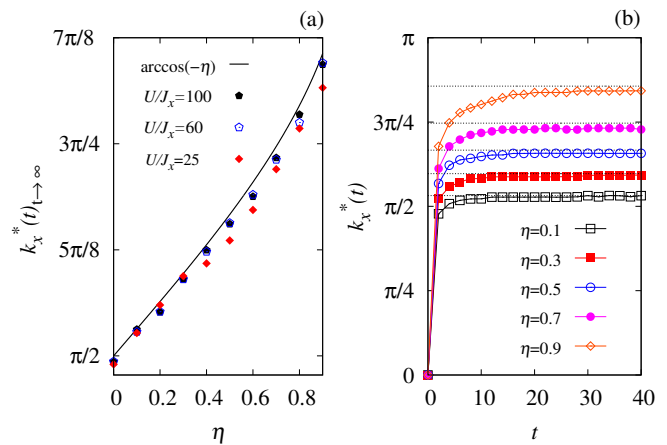


FIG. 4. (Color online) (a) Location of the momentum peak k_x^* after a long expansion time obtained from the mean-field calculation as a function of the hopping ratio η , for $U/J_x = 25, 60$, and 100 (points). The prediction of Eq. (13) is depicted as a solid line. (b) The time evolution of the location of the momentum peak for $U/J_x = 60$ and several values of η . The horizontal dashed-dotted lines show the values predicted in Eq. (13). The time is reported in units of \hbar/J_x .

for small values η . The largest deviations, for all values of U/J_x , are observed for the largest values of η . This occurs because as η is increased, the superfluid wings surrounding the Mott insulator increase their size; as a result, the total kinetic energy is lower than that of the Mott insulator, and one of our assumptions ($E_{\text{kin}} \approx 0$) starts to fail. Nevertheless, as Fig. 4(a) shows, for the largest values of η , the differences are still relatively small even for the smallest values of U/J_x that support a Mott insulator. They also can be seen to decrease when increasing U/J_x . For $U/J_x = 100$, the results are barely distinguishable from the analytic results for the hard-core limit. Overall, the fact that only for large values of U/J_x one can realize a Mott insulator in the initial state allows for the hard-core description to be a good approximation in all cases analyzed here.

We conclude this section by showing, in Fig. 4(b), results for the location of the momentum peak as function of time, for $U/J_x = 60$. That figure makes clear that, as time passes, the location of the peak rapidly approaches the values predicted by Eq. (13) (dotted horizontal lines). It also shows that it takes a shorter time to reach those values for smaller values of η . In our calculations, the value of k_x^* is determined as the local center of mass of the momentum distribution function around the position of the brightest peak.

V. EXPANSION IN ALL DIRECTIONS

We now examine the situation in which the initial Mott insulator is allowed to expand in all directions. For such a case, we consider $V_x = V_y = V$ and $J_x = J_y = J$. We

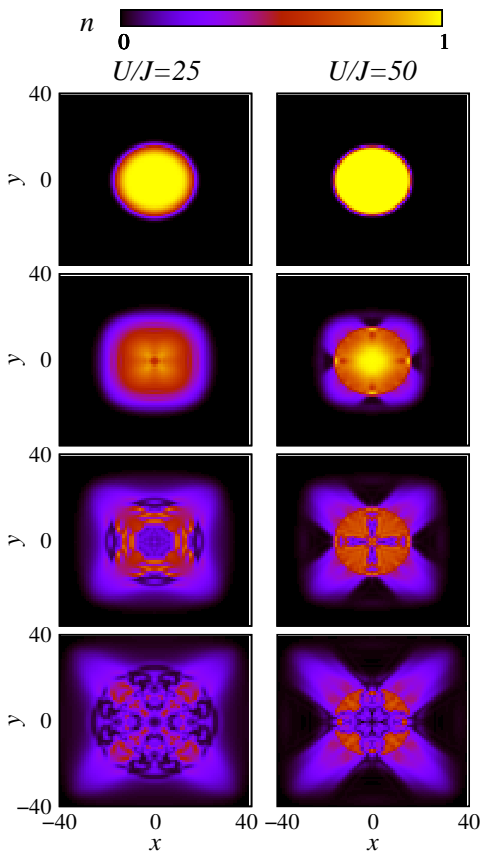


FIG. 5. (Color online) Comparison between the time evolution of the density profile across the trap of systems with $U/J = 25$ (left) and $U/J = 50$ (right), at $t = 0, 4, 8$, and 12 (from top to bottom) following the release from traps with $V/J = 0.053$ and $V/J = 0.161$, respectively. The time is reported in units of \hbar/J .

turn off the trap at $t = 0$, and study the time evolution of the density and momentum distribution for systems with $U/J = 25, 30, 40, 50, 60, 80$, and 100 . Note that the Mott insulator can only be achieved in systems with large enough values of U/J ($U/J \gtrsim 23.2$ within the mean-field approach in 2D).

Figure 5 depicts the time evolution of the density profile of the expanding bosons with $U/J = 25$ (left) and $U/J = 50$ (right). Interestingly, although the rightmost case has an interaction energy that is twice that of the leftmost one, the expansion is somehow similar in both cases. At the moment the trap is turned off ($t = 0$), the Mott-insulator domain is easily discernible from the superfluid one surrounding it. The lattice sites in the vicinity of the center of the system have unit occupancies and are surrounded by a thin ring with density smaller than one. Note that, as expected from the way we construct the initial state (see Sec. III), the superfluid ring in the system with $U/J = 50$ is smaller than the one in the system with $U/J = 25$.

After turning off the trap, the bosonic cloud expands and the Mott insulator melts. In Fig. 5, it is remarkable

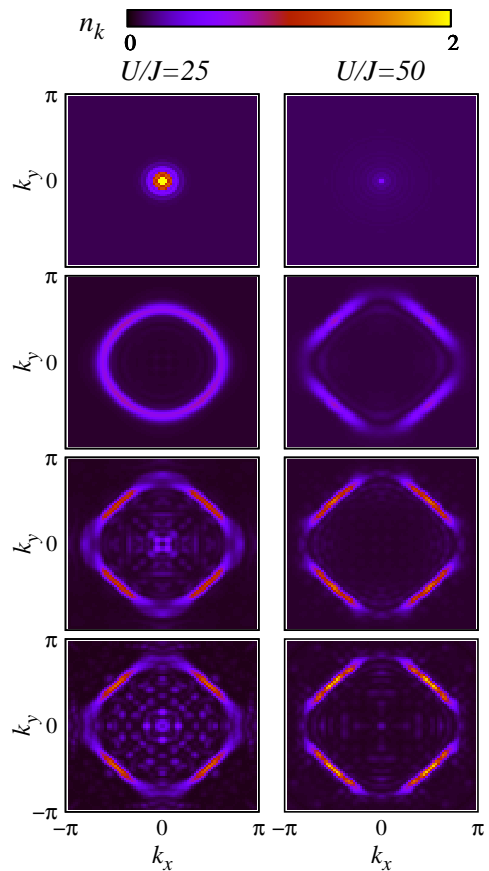


FIG. 6. (Color online) Comparison between the time evolution of the momentum distribution function of systems with $U/J = 25$ (left) and $U/J = 50$ (right), at $t = 0, 4, 8$, and 12 (from top to bottom) following the release from traps with $V/J = 0.053$ and $V/J = 0.161$, respectively. The time is reported in units of \hbar/J .

that the expansion along the diagonals is always faster than that along the x and y axes. This leads to a square-like density profile for $t > 0$. Such a behavior is accentuated as U/J increases, as seen in the right panels in Fig. 5, where the expansion occurs almost entirely along the diagonals.

The evolution of the momentum distribution function, corresponding to the density profiles depicted in Fig. 5, is shown in Fig. 6. At $t = 0$, peaks can be seen in the center of the momentum distribution function. They correspond to the bosons that are in the superfluid rings surrounding the Mott insulator. The difference between the size of those rings for $U/J = 25$ (Fig. 5, left) and $U/J = 50$ (Fig. 5, right) is apparent in the initial momentum distribution, as the height of the peak for the $U/J = 25$ case is significantly larger than that in the $U/J = 50$ case. Surprisingly, for $t > 0$, these peaks rapidly evolve into circular-like structures, which in turn, become square-like as time passes (Fig. 6). The initial ring structure is less evident in the $U/J = 50$ case at $t = 4$ because the formation of the square-like struc-

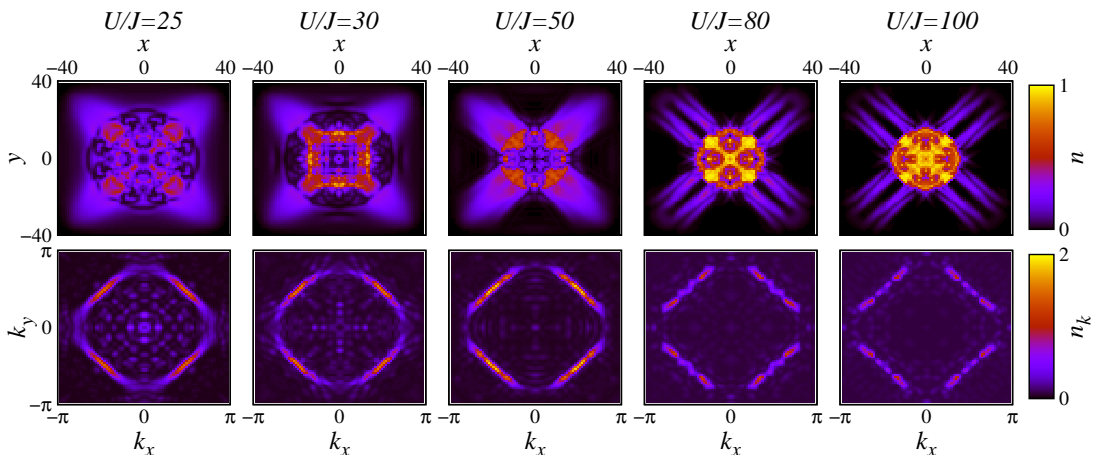


FIG. 7. (Color online) Top row: Comparison between the density profiles of systems with $U/J = 25, 30, 50, 80,$ and 100 (from left to right), at $t = 12$ following the release from traps with $V/J = 0.053, 0.0764, 0.161, 0.278$ and 0.356 , respectively. Bottom row: Corresponding momentum distribution functions. The time is reported in units of \hbar/J .

ture occurs faster as the value of U/J is increased. Also, the structure discernible in the momentum distribution function for small values of k_x and k_y (bottom panels for $U/J = 25$) disappears as the value of U/J is increased (see how much weaker it is in bottom panels for $U/J = 50$) and most of the bosons have momenta that lay within the edges of the square. The existence of this structure, in which bosons remain with small values of k_x and k_y , can be directly related to the size of the initial superfluid domain, which, as said before, decreases as the system approaches the hard-core limit.

A comparison between the density and momentum distributions of systems with different values of U/J ($U/J = 25, 30, 50, 80,$ and 100), at the time the bosons reach the boundaries of our 80×80 lattice ($t = 12$), is presented in Fig. 7. These plots make evident that the expansion mainly occurs along the diagonals as U/J increases and, at the same time, the momentum distribution function acquires a clearer square shape.

An understanding of the behavior exhibited by these systems, when allowed to expand in all directions, can be gained following a similar line of reasoning as done in the previous section. If $U/J \gg 1$, a good description is provided by the hard-core boson picture. For hard-core bosons, after the trapping potential is turned off, the total energy is the kinetic energy, just as in the expansion in one direction. The dispersion relation $\epsilon_{\mathbf{k}}$ in the isotropic case reduces to

$$\epsilon_{\mathbf{k}} = -2J(\cos k_x + \cos k_y). \quad (14)$$

We now assume, once again to simplify the argument, that the system before the expansion is a perfect Mott insulator, i.e., all the particles are localized in their respective sites, and occupy all possible momenta in \mathbf{k} space. Therefore, the kinetic energy is again $E_{\text{kin}} = 0$, and it is conserved during the expansion. Furthermore, let us assume that, after long time, the majority of bosons will occupy (“condense” to) modes with particular \mathbf{k} vectors

(as seen in the mean-field calculations). Energy conservation is guaranteed by the assumption that the energy of each occupied mode vanishes. Under those assumptions, the \mathbf{k} vector of the modes populated by the bosons can be calculated from the dispersion relation as

$$\epsilon_{\mathbf{k}} = -2J(\cos k_x + \cos k_y) = 0. \quad (15)$$

The solution to this equation is given by the square-like contour plot seen in Fig. 8, for the case with $w = 0$. Analytically, such a contour plot is described by the expressions

$$k_y = \pi \pm k_x, \quad k_y = -\pi \pm k_x. \quad (16)$$

Remarkably, the momentum distribution of all systems in Fig. 7 has converged to a distinctive square-like structure. It closely resembles the prediction of Eq. (16), as represented in Fig. 8. The deviations from the exact results in Eq. (16) can be understood to be the result of (i) the finite values of U/J in all our calculations, and (ii) the fact that the Mott-insulating domains with $n = 1$ are always surrounded by superfluid ones. Once again, the first modifies the dispersion relation in Eq. (14), and the second one reduces the energy from the value assumed in Eq. (15). As clearly seen in Fig. 7, when U/J increases and the superfluid domains in the initial state reduce their size, the momentum distribution becomes closer to the square-like contour defined in Eq. (16). The robustness of the results, despite points (i) and (ii) above, is remarkable. Hence we expect that they should be reproducible in experiments with ultracold bosons even at finite, but low, temperatures.

The analysis above also allows one to understand the expansion pattern seen in the density profiles in Figs. 5 and 7. The density profiles for $t > 0$ are determined by the velocities with which bosons expand across the lattice. In the hard-core limit, the group velocity is

$$\mathbf{v}_g = \nabla \epsilon_{\mathbf{k}} = 2J(\sin k_x \hat{x} + \sin k_y \hat{y}), \quad (17)$$

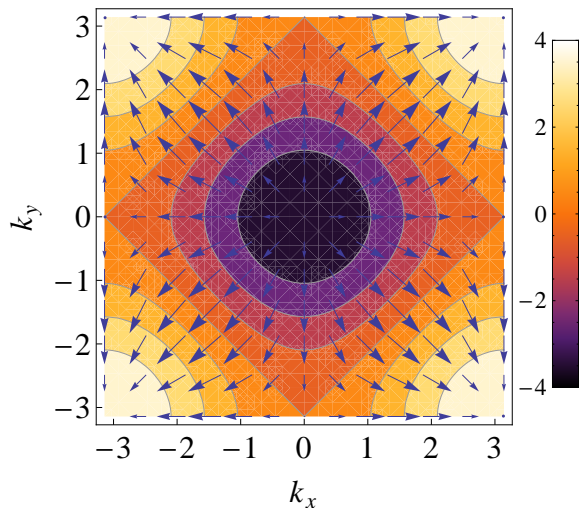


FIG. 8. (Color online) Depiction of the group velocity vector field, given by Eq. (17) in k -space, along with a series of contour plots satisfying the equation $-2(\cos k_x + \cos k_y) = w/J$, where $w/J = -2, -1.5, -1, -0.5, 0, 0.5, 1, \text{ and } 2$.

which produces the vector field plot seen in Fig. 8. It is clear that the group velocities, which are perpendicular to the contour plots, increase in magnitude for those k modes along the diagonal. (The maximum group velocity occurs when $\epsilon_{\mathbf{k}} = 0$ along the diagonal.) Therefore, if such modes are highly populated, the net effect is that the system will expand preferably along the directions indicated by those group velocity vectors. Indeed, the high population of such modes is apparent in the momentum distribution functions depicted in Fig. 7. The low population of the modes in the vertices of the square indicates the suppression of particles with momenta close to $(\pm\pi, 0)$ and $(0, \pm\pi)$, which have vanishing group velocities. In Fig. 7, the accuracy of this description can be seen to improve with increasing U/J . It is interesting to note that the system expands at the greatest speed possible by populating the modes with the highest group velocity that are consistent with the conservation of the energy, as can be concluded from the momentum distributions and comparing them with the analytical results.

We have already shown that, during the expansion from a mostly Mott-insulating state, bosons tend to populate momentum modes around well-defined values. Results have been presented for mean-field calculations and supported by analytic arguments. One can now wonder whether all these highly populated modes are coherently coupled forming a simple Bose-Einstein condensate, or whether they are part of fragmented condensates, or quasicondensates, or their occupation is simply $O(N_b^0)$ but their number increases with increasing system size. In strongly correlated systems, it is possible that modes with different momenta couple to each other and still form a simple Bose-Einstein condensate.

In the presence of interactions, condensation can be understood as effective single-particle states (natural or-

bitals) being macroscopically populated. Following Penrose and Onsager [50], one needs to diagonalize the one-particle density matrix $\rho_{i,j}$ and study its eigenvalues λ_η

$$\sum_j \rho_{i,j} \varphi_j^\eta = \lambda_\eta \varphi_i^\eta. \quad (18)$$

(i) If only one of them scales proportionally to the total number of bosons in the system (N_b), one has simple Bose-Einstein condensation. (ii) If more than one of them scales proportionally to N_b , this means that fragmentation occurs [51]. (iii) One can also have many of them that scale proportionally to N_b^α ($0 < \alpha < 1$), and one would then say that quasicondensation occurs. (iv) Finally, if all of them scale as $O(N_b^0)$, the system does not exhibit Bose-Einstein condensation or quasicondensation. Interestingly, exact results for expanding hard-core bosons in one dimension [16] have already shown that the largest eigenvalue of the one-particle density matrix in a system out of equilibrium can diverge ($\propto \sqrt{N_b}$ in that case), while still being composed by bosons with many different momenta. In those systems, there were as many populated momenta as those available in the Fermi sea of the noninteracting fermions to which hard-core bosons were mapped.

Within the mean-field approximation, the elements of the one-particle density matrix reduce to

$$\rho_{i,j} = \Phi_i^* \Phi_j + \delta_{i,j} (n_i - |\Phi_i|^2). \quad (19)$$

The expression in Eq. (19), which holds because of the intrinsic form of the Gutzwiller state in Eq. (2), implies that the one-particle density matrix can only attain at most one eigenvalue which grows as the total number of particles grows; thus if fragmentation or quasicondensation occurs in a real system, the Gutzwiller mean-field approach will fail to reproduce them [52]. A scenario in which all λ 's are $O(N_b^0)$, on the other hand, can of course be reproduced by this approximation (e.g., the Mott insulator at zero temperature and the normal phase at high temperature).

In Fig. 9, we show the time evolution of the largest eigenvalue λ_0 of $\rho_{i,j}$ for three different values of U/J ($U/J = 25, 50, \text{ and } 100$) in our systems. Due to the presence of the superfluid rings in the initial state, λ_0 is not always small at $t = 0$. (As expected, its value at $t = 0$ decreases as U/J is increased.) For all the systems studied in this work, we find that the occupation of the highest populated natural orbital always grows during the expansion (Fig. 9), while the occupation of the other natural orbitals remains negligible at all times. In addition, we have verified that λ_0 always increases proportionally to the total number of particles. Hence, at least within the mean-field approximation, we find that one natural orbital is macroscopically populated. This means that one of the scenarios (i)-(iii) could be relevant to the physics of the real systems. Experiments and/or other theoretical approaches will need to be used to identify which of those scenarios (if any) is the correct one.

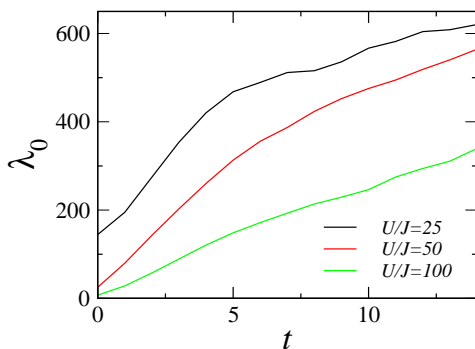


FIG. 9. (Color online) Comparison between the time evolution of the occupation of the highest populated natural orbital λ_0 for systems with $U/J = 25$ (black), $U/J = 50$ (red), and $U/J = 100$ (green), after turning off traps with $V/J = 0.053$, 0.162 , and 0.356 , respectively. The time is reported in units of \hbar/J .

VI. CONCLUSIONS

We have presented a detailed study of the expansion of $n = 1$ bosonic Mott insulators in two-dimensional optical lattices. In all cases studied here, the initial states were prepared in such a way that the largest fraction possible of the bosons would be part of the Mott-insulating domain. Two setups were considered: the expansion along one direction of an anisotropic system, which was initially trapped only along the x direction, and the expansion of an isotropic system, which was allowed to expand in all directions. In the first case, we have shown that the expansion of the Mott insulator leads to a high population of two well-defined momentum states. Those momenta were found to be controlled by the ratio of the hopping amplitudes along the x and y directions. In the second case, the expansion of a Mott insulator in all directions produced a simple condensate composed by bosons with many different momenta. Given the approximated nature of our calculations, experiments, and/or unbiased

theoretical work, will need to verify our findings and address the nature of the condensation seen within the Gutzwiller mean-field approximation. For the two set ups mentioned before, we also presented analytical arguments to determine which momentum modes are populated during the expansion.

It is important to notice that the phenomena we have observed here arise because of a subtle interplay between quantum tunneling and strong correlations. Both effects play a crucial role in the generation of the condensates as, on the one hand, tunneling is necessary for the system to expand, and on the other hand, interactions are necessary for the bosons to redistribute the energy and couple coherently. In the absence of interactions, the system still expands, but the momentum distribution remains unchanged from its initial value, i.e., it remains featureless if one starts from purely localized particles in the lattice sites (a Fock state), and no condensation occurs.

Finally, our study supports the conclusion in Ref. [26], and generalizes it to the soft-core boson case, that strongly correlated atom lasers can be generated from the expansion of Mott-insulating states. Furthermore, after the results in Sec. IV, one can see that the momenta of those matter waves can be controlled by changing the ratio between the hopping parameters in the different directions in the lattice. In addition, if one cannot change those, in an isotropic lattice (Sec. V), the momenta of the lasers can be controlled by changing the direction along which the Mott insulator is allowed to expand. In the latter setup, the best results would be obtained by constraining the Mott insulator to expand along the diagonals in the lattice.

ACKNOWLEDGMENTS

This work was supported by the U.S. Office of Naval Research.

-
- [1] I. Bloch, J. Dalibard, and W. Zwerger, *Rev. Mod. Phys.* **80**, 885 (2008).
 - [2] M. A. Cazalilla, R. Citro, T. Giamarchi, E. Orignac, and M. Rigol, arXiv:1101.5337 (2011), To be published in *Rev. Mod. Phys.*
 - [3] M. Greiner, O. Mandel, T. Esslinger, T. W. Hänsch, and I. Bloch, *Nature* **415**, 39 (2002).
 - [4] I. B. Spielman, W. D. Phillips, and J. V. Porto, *Phys. Rev. Lett.* **98**, 080404 (2007).
 - [5] T. Stöferle, H. Moritz, C. Schori, M. Köhl, and T. Esslinger, *Phys. Rev. Lett.* **92**, 130403 (2004).
 - [6] M. Greiner, O. Mandel, T. W. Hänsch, and I. Bloch, *Nature* **419**, 51 (2002).
 - [7] T. Kinoshita, T. Wenger, and D. S. Weiss, *Nature* **440**, 900 (2006).
 - [8] S. Hofferberth, I. Lesanovsky, B. Fischer, T. Schumm, and J. Schmiedmayer, *Nature* **449**, 324 (2007).
 - [9] C.-L. Hung, X. Zhang, N. Gemelke, and C. Chin, *Phys. Rev. Lett.* **104**, 160403 (2010).
 - [10] S. Trotzky, Y.-A. Chen, A. Flesch, I. P. McCulloch, U. Schollwöck, J. Eisert, and I. Bloch, *Phys. Rev. Lett.* **106**, 155302 (2011).
 - [11] J. Dziarmaga, *Advances in Physics* **59**, 1063 (2010).
 - [12] M. A. Cazalilla and M. Rigol, *New J. Phys.* **12**, 055006 (2010).
 - [13] A. Polkovnikov, K. Sengupta, A. Silva, and M. Vengalattore, *Rev. Mod. Phys.* **83**, 863 (2011).
 - [14] F. Dalfovo, S. Giorgini, L. P. Pitaevskii, and S. Stringari, *Rev. Mod. Phys.* **71**, 463 (1999).
 - [15] B. Sutherland, *Phys. Rev. Lett.* **80**, 3678 (1998).
 - [16] M. Rigol and A. Muramatsu, *Phys. Rev. Lett.* **94**, 240403 (2005).

- [17] A. Minguzzi and D. M. Gangardt, *Phys. Rev. Lett.* **94**, 240404 (2005).
- [18] F. Heidrich-Meisner, S. R. Manmana, M. Rigol, A. Muramatsu, A. E. Feiguin, and E. Dagotto, *Phys. Rev. A* **80**, 041603(R) (2009).
- [19] M. P. A. Fisher, P. B. Weichman, G. Grinstein, and D. S. Fisher, *Phys. Rev. B* **40**, 546 (1989).
- [20] M. Rigol and A. Muramatsu, *Phys. Rev. Lett.* **93**, 230404 (2004).
- [21] M. Rigol and A. Muramatsu, *Mod. Phys. Lett.* **19**, 861 (2005).
- [22] K. Rodriguez, S. R. Manmana, M. Rigol, R. M. Noack, and A. Muramatsu, *New J. Phys.* **8**, 169 (2006).
- [23] J. Lancaster and A. Mitra, *Phys. Rev. E* **81**, 061134 (2010).
- [24] F. Heidrich-Meisner, M. Rigol, A. Muramatsu, A. E. Feiguin, and E. Dagotto, *Phys. Rev. A* **78**, 013620 (2008).
- [25] U. Schollwöck, *Rev. Mod. Phys.* **77**, 259 (2005).
- [26] I. Hen and M. Rigol, *Phys. Rev. Lett.* **105**, 180401 (2010).
- [27] L.-K. Lim, C. M. Smith, and A. Hemmerich, *Phys. Rev. Lett.* **100**, 130402 (2008).
- [28] M. Di Liberto, O. Tieleman, V. Branchina, and C. Morais Smith, *Phys. Rev. A* **84**, 013607 (2011).
- [29] D. Jaksch, C. Bruder, J. I. Cirac, C. W. Gardiner, and P. Zoller, *Phys. Rev. Lett.* **81**, 3108 (1998).
- [30] G. G. Batrouni, R. T. Scalettar, and G. T. Zimanyi, *Phys. Rev. Lett.* **65**, 1765 (1990).
- [31] J. K. Freericks and H. Monien, *Phys. Rev. B* **53**, 2691 (1996).
- [32] N. Elstner and H. Monien, *Phys. Rev. B* **59**, 12184 (1999).
- [33] T. D. Kühner, S. R. White, and H. Monien, *Phys. Rev. B* **61**, 12474 (2000).
- [34] B. Capogrosso-Sansone, N. V. Prokof'ev, and B. V. Svistunov, *Phys. Rev. B* **75**, 134302 (2007).
- [35] B. Capogrosso-Sansone, S. G. Söyler, N. V. Prokof'ev, and B. V. Svistunov, *Phys. Rev. A* **77**, 015602 (2008).
- [36] G. G. Batrouni, V. Rousseau, R. T. Scalettar, M. Rigol, A. Muramatsu, P. J. H. Denteneer, and M. Troyer, *Phys. Rev. Lett.* **89**, 117203 (2002).
- [37] S. Wessel, F. Alet, M. Troyer, and G. G. Batrouni, *Phys. Rev. A* **70**, 053615 (2004).
- [38] M. Rigol, G. G. Batrouni, V. G. Rousseau, and R. T. Scalettar, *Phys. Rev. A* **79**, 053605 (2009).
- [39] S. Fölling, A. Widera, T. Müller, F. Gerbier, and I. Bloch, *Phys. Rev. Lett.* **97**, 060403 (2006).
- [40] G. K. Campbell, J. Mun, M. Boyd, P. Medley, A. E. Leanhardt, L. G. Marcassa, D. E. Pritchard, and W. Ketterle, *Science* **313**, 649 (2006).
- [41] N. Gemelke, X. Zhang, C.-L. Hung, and C. Chin, *Nature* **460**, 995 (2009).
- [42] W. S. Bakr, A. Peng, M. E. Tai, R. Ma, J. Simon, J. I. Gillen, S. Fölling, L. Pollet, and M. Greiner, *Science* **329**, 547 (2010).
- [43] J. F. Sherson, C. Weitenberg, M. Endres, M. Cheneau, I. Bloch, and S. Kuhr, *Nature* **467**, 68 (2010).
- [44] K. Sheshadri, H.R. Krishnamurthy, R. Pandit, T.V. Ramakrishnan, *Europhys. Lett.* **22**, 257 (1993).
- [45] L. Amico and V. Penna, *Phys. Rev. Lett.* **80**, 2189 (1998).
- [46] D. Jaksch, V. Venturi, J. I. Cirac, C. J. Williams, and P. Zoller, *Phys. Rev. Lett.* **89**, 040402 (2002).
- [47] J. Zakrzewski, *Phys. Rev. A* **71**, 043601 (2005).
- [48] M. Snoek, *Europhys. Lett.* **95**, 30006 (2011).
- [49] S. Sachdev, *Quantum Phase Transitions*, Cambridge University Press, 2000.
- [50] O. Penrose and L. Onsager, *Phys. Rev.* **104**, 576 (1956).
- [51] A. J. Leggett, *Rev. Mod. Phys.* **73**, 307 (2001).
- [52] M. Buchhold, U. Bissbort, S. Will, and W. Hofstetter, *Phys. Rev. A* **84**, 023631 (2011).